

Article

Nanocomposites of Copper Trimesinate and Graphene Oxide as Sorbents for the Solid-Phase Extraction of Organic Dyes

Igor E. Uflyand , Victoria N. Naumkina and Vladimir A. Zhinzhilo

Department of Chemistry, Southern Federal University, 344090 Rostov-on-Don, Russia;
vnaumkina@sfnedu.ru (V.N.N.); i06993@yandex.ru (V.A.Z.)

* Correspondence: ieuflyand@sfnedu.ru; Tel.: +7-928-111-2880

Abstract: A nanocomposite based on graphene oxide and copper trimesinate was obtained by the in situ method. The samples have permanent porosity and a microporous structure with a large surface area corresponding to the adsorption type I. A study of the adsorption properties of the obtained composites with respect to organic dyes (malachite green, indigo carmine, brilliant green, Rose Bengal, crystal violet) showed that adsorption largely depends on the content of graphene oxide in the composites. The complex is an effective sorbent for the extraction of cationic and neutral organic dyes when the content of graphene oxide in the nanocomposite is 20% of the calculated copper trimesinate due to electrostatic forces of interaction. For anionic dyes, the maximum adsorption is achieved when using a composite containing 5% graphene oxide due to the predominance of physical sorption. Experimental results show that the obtained sorbent can be used for extraction in a wide pH range, illustrating the excellent pH window offered by this adsorbent. Kinetics data were properly fitted with the pseudo-second-order model. Equilibrium data were best correlated with the Freundlich model. The process was endothermic and spontaneous in nature. The composite makes it possible to achieve a maximum sorption of 393 mg/g, which is a sufficiently high value for the absorption of dyes.

Keywords: composites; copper trimesinate; solid-phase extraction; graphene oxide; pollutants



Citation: Uflyand, I.E.; Naumkina, V.N.; Zhinzhilo, V.A. Nanocomposites of Copper Trimesinate and Graphene Oxide as Sorbents for the Solid-Phase Extraction of Organic Dyes. *J. Compos. Sci.* **2022**, *6*, 215. <https://doi.org/10.3390/jcs6070215>

Academic Editor: Jian-Zhang Chen

Received: 28 June 2022

Accepted: 17 July 2022

Published: 20 July 2022

Publisher's Note: MDPI stays neutral with regard to jurisdictional claims in published maps and institutional affiliations.



Copyright: © 2022 by the authors. Licensee MDPI, Basel, Switzerland. This article is an open access article distributed under the terms and conditions of the Creative Commons Attribution (CC BY) license (<https://creativecommons.org/licenses/by/4.0/>).

1. Introduction

Organic dyes, widely used in the printing, textile, paper, paint and varnish industries and in the plastics industry, are recognized manufactured pollutants that can slow down and change the chemistry of the photosynthesis cycle. In addition, they contribute to the destabilization of metabolic reactions in plant organisms and can cause mutagenic and carcinogenic diseases in humans and animals [1–4]. Among the developed methods for the removal of dyes from wastewater, ion-exchange filtration [5], membrane filtration [6], chemical oxidation [7], photocatalysis [8–10], catalytic degradation [11,12], electrochemical oxidation [13,14], biodegradation [15,16] and coagulation/flocculation [17–19] should be noted. The main disadvantages of most traditional methods are a low selectivity, a low rate of decomposition of dyes and a high energy consumption [20,21]. The adsorption is the most efficient, cheap, flexible, applicable, compatible, eco-friendly, operable, rapid, reusable and widely used technique compared to other methods for removing organic dyes [22]. Therefore, researchers have devoted considerable attention to the search for new adsorbents as advanced materials for the effective removal of dyes.

In recent decades, the attention of scientists has been focused on a class of polyfunctional materials called metal-organic frameworks (MOFs), which can be used as solid-state adsorbents for organic dyes [23]. They are characterized by a high chemical resistance and a significant specific internal surface hundreds of times greater than carbon materials (up to 10,000 m²/g). Among the various MOFs, MOFs such as Cu₃(BTC)₂(H₂O)₃·xH₂O (where H₃BTC = 1,3,5-benzenetricarboxylic or trimesic acid) containing the binuclear Cu(II)

paddlewheel structures are of particular interest for testing the adsorption capacity. This MOF was first synthesized in 1999 [24] and designated as HKUST-1 (Hong Kong University of Science and Technology) or MOF-199. It has a high specific surface area and an interconnected 3D pore system with pore sizes of $9 \text{ \AA} \times 9 \text{ \AA}$ [25,26]. Various Cu–BTC complexes were studied, including $\text{Cu}_3(\text{BTC})_2 \cdot 3\text{H}_2\text{O}$ [27,28], $\text{Cu}_2(\text{OH})(\text{BTC})(\text{H}_2\text{O})_2 \cdot n\text{H}_2\text{O}$ [29] and $\text{Cu}(\text{BTC}-\text{H}_2)_2(\text{H}_2\text{O})_2 \cdot 3\text{H}_2\text{O}$ [30].

However, MOFs have some limitations associated with high selectivity, easily lose their adsorption activity in a humid atmosphere and are difficult to post-synthetic functionalize. To expand the practical application of MOFs, a promising approach is to create their composites with other materials, which makes it possible to obtain polyfunctional materials with improved technological properties, which, in addition to the physical sorption provided by the network structure of MOFs, retain adsorbate molecules using chemisorption processes. Such materials are graphene-based compounds, since separated and functionalized graphene sheets will increase dispersion interactions, while MOFs will increase the pore space in which adsorbates can be stored [31,32].

The purpose of the work was to obtain a nanocomposite material based on a copper(II) trimesinate and graphene oxide (GO) and to study the possibilities of such a material for the solid-phase extraction of organic dyes. The objectives of the study were the synthesis of a hybrid composite material based on copper trimesinate and GO, the selection of MOF:GO ratios to obtain the most effective material, the study of the ability of the obtained material regarding the solid-phase extraction of model pollutants and the study of the influence of various variables (pH, initial dye concentration, temperature and contact time) on the process of solid-phase extraction.

2. Materials and Methods

2.1. Materials

Methanol (MeOH, 99.9%), ethanol (EtOH, 98%) and methylene chloride were supplied by Sigma-Aldrich (Moscow, Russia); the purity of the solvents was determined by selective gas chromatography. Copper(II) sulfate pentahydrate ($\text{CuSO}_4 \cdot 5\text{H}_2\text{O}$, $\geq 99.0\%$), 1,3,5-benzenetricarboxylic acid (H_3BTC , 95.0%), NaOH, H_2SO_4 , NaNO_3 , KMnO_4 and H_2O_2 were purchased from Sigma-Aldrich (Moscow, Russia) and used without further purification. As a starting material, we used S-1 flaky graphite (technical grade, Lenreaktiv, Russia) without additional purification. The graphite particle size was 125–1000 μm (mean size 200 μm).

2.2. Characterization Techniques

The Fourier transform IR (FTIR) spectra were taken with a Perkin Elmer Spectrum 100 FTIR spectrometer (Perkin Elmer) from KBr pellets, using SoftSpectra software for the data analysis (Shelton, CT). Scanning electron microscopic (SEM) images were taken with a ZEISS Crossbeam 340 device (Carl Zeiss) at an accelerating voltage of 3 kV. Secondary electrons were detected with an Everhart-Thornley detector (SE2). The distribution of chemical elements on the surface of the samples was determined by X-ray energy dispersive microanalysis (EDX) on an Oxford X-max 80 microanalyzer with an electron probe energy of $\leq 10 \text{ keV}$. The nitrogen adsorption/desorption experiments were performed at 77 K (liquid N_2) using the AUTOSORB-1 system (Quantachrome, Boynton Beach, FL, USA) by the static volumetric method; before the analysis, the samples were degassed by heating at 150 °C for 12 h in vacuum. The Brunauer–Emmett–Teller surface area (S_{BET}) was obtained from the amount of N_2 physically sorbed at various relative pressures (P/P_0) based on the linear part of the six-point adsorption data at $P/P_0 = 0.02\text{--}0.10$. The total pore volume (V_{total}) was calculated by the Horvath Kawazoe method at $P/P_0 = 0.99$. The micropore volume (V_{micro}) was obtained by the Barrett–Joyner–Halenda adsorption and the t-plot methods, respectively. To assess the adsorption capacity, ultrahigh purity gases (99.995%) were used.

2.3. Synthesis of the Sorbent

The composite was synthesized in situ in two stages: obtaining GO by the modified Hummers method, and the subsequent introduction of copper trimesinate into the synthesis procedure.

2.3.1. Synthesis of Graphene Oxide

GO was prepared by the Hummers method [33] in accordance with the previously developed protocol [34]. A total of 15 g of finely ground sodium nitrate powder was added to 115 mL of concentrated sulfuric acid at a temperature not exceeding 0 °C. The mixture was stirred until completely dissolved. A total of 5 g of crushed graphite was added to the mixture, stirred until homogeneous and then carefully oxidized, introducing 15 g of potassium permanganate in small portions so that the temperature does not rise above 20 °C. Then, 230 mL of distilled water was added in small portions, making sure that the temperature of the system does not exceed 98 °C. The rest of the potassium permanganate is reduced with a concentrated solution of hydrogen peroxide. As a result, a thin suspension of GO in water was obtained, stable for a month (Figure 1). GO was purified by dialysis.



Figure 1. Suspension of GO in water.

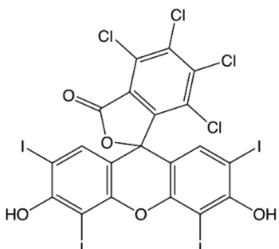
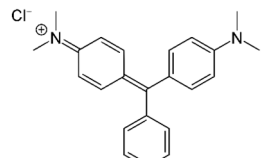
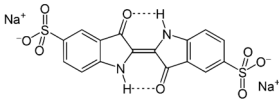
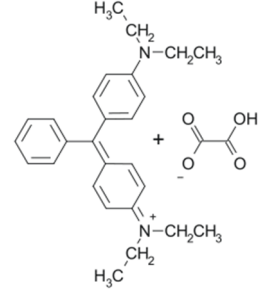
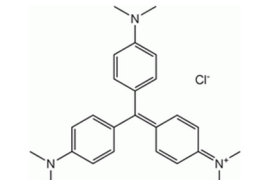
2.3.2. Synthesis of Nanocomposite

First, a soluble form of 1,3,5-benzenetricarboxylic acid is prepared as the sodium salt. Then, 3.48 g (0.0166 mol) of 1,3,5-benzenetricarboxylic acid was added to an aqueous solution containing 1.98 g of sodium hydroxide (in 200 mL of water) while heating to 80 °C. Then, 0.25 g of GO and an aqueous solution of 6.22 g (0.0250 mol) of copper sulfate are added to the resulting solution of sodium trimesinate. The precipitate that formed was sonicated in distilled water (60 W, 40 kHz) for 24 h, filtered off and dried in air. At the final stage, it is sequentially kept in absolute alcohol and then in dry ethyl acetate and dichloromethane. The exposure in each solvent was 8 h. At the end of the procedure, the precipitate was centrifuged, washed with dry dichloromethane and dried for 10 h in a dynamic vacuum at 120 °C. GO was introduced into the composite in an amount of 5 wt.% of the calculated copper trimesinate. The yield was 4.56 g (91.23% in terms of copper trimesinate). Similarly, the synthesis of the composite was conducted in the amounts of 10 and 20 wt.% GO of the calculated copper trimesinate. The yield was 4.85 g and 4.74 g (96.90% and 94.71% in terms of copper trimesinate, respectively).

2.4. Dye Adsorption Study

In this work, serial adsorption experiments were conducted to remove dyes from aqueous solutions by using the synthesized sorbents. The following dyes were studied in the work: malachite green (MG), indigo carmine (IC), brilliant green (BG), Rose Bengal (RB) and crystal violet (CV) (Table 1). The dye stock solutions were prepared by dissolving precisely weighed dye powders in distilled water to a concentration of 40 mg/L. Experimental solutions were obtained by diluting the initial dye solution in exact proportions to the required initial concentrations.

Table 1. Studied dyes.

Name	Molecular Structure	λ_{\max} (nm)	Ref.
RB		546	[35]
MG		617	[36,37]
IC		610 (600)	[37]
BG		625	[38,39]
CV		590 (594)	[40]

2.4.1. Study of the Dependence of Sorption on the Initial Dye Concentration

Solutions of dyes with a volume of 40 mL and with concentrations of 20, 10, 5, 2.5 and 1.25 mg/L were placed in a 100 mL beaker and thermostated at 278, 293 and 308 K on a magnetic stirrer, adjusting the rotation speed so that the mixing was effective but air was not drawn into the liquid phase. When the solutions reached a predetermined temperature, a 10 mg sorbent was introduced. Upon reaching 3 h, 10 mL of the sorbent suspension was taken from each dye solution and subjected to centrifugation for 5 min. The residual dye concentration was determined in the filtrate by using a spectrophotometer at specific wavelengths for each dye.

The adsorption capacities (q (mg/g)) were evaluated by the following equations:

$$q_t = (C_0 - C_t)V/m \quad (1)$$

$$q_e = (C_0 - C_e)V/m \quad (2)$$

where q_t and q_e are the dye amount (mg/g) adsorbed on the sorbent at time t and in equilibrium, respectively; C_0 , C_t and C_e are the dye concentrations in the solution (mg/L) at the initial stage at time t and in equilibrium, respectively; m (g) and V (L) are the sorbent dosage and the volume of the dye solution, accordingly.

The degree of adsorption R (%) (extraction ratio of the sorbate) was calculated by the formula:

$$R (\%) = (C_0 - C_e)/C_0 \times 100\% \quad (3)$$

The data obtained during the experiment were analyzed using the Langmuir and Freundlich models.

2.4.2. Study of the Dependence of Sorption on Contact Time

Solutions of dyes with a volume of 40 mL and with a concentration of 20 mg/L were placed in a 100 mL beaker and thermostated at 278, 293 and 308 K on a magnetic stirrer, adjusting the rotation speed so that the mixing was effective but air was not drawn into the liquid phase. When the solutions reached a predetermined temperature, a 20 mg sorbent was introduced, and a timer was started. Every 5, 10, 15, 30, 45 and 60 min, 10 mL of the sorbent suspension was taken from each dye solution and subjected to centrifugation for 5 min. The residual dye concentration was determined in the filtrate by using a spectrophotometer at specific wavelengths for each dye.

The data obtained during the study of the adsorption process were analyzed using kinetic models of pseudo-first and pseudo-second order reactions [41,42]. The pseudo-first order rate equation is:

$$\ln(q_e - q_t) = \ln q_e - k_1 t, \quad (4)$$

where k_1 (min^{-1}) is the adsorption rate constant of the pseudo first order model.

The differential form of the classical pseudo-second order rate equation is:

$$\frac{dq_t}{dt} = k_2(q_e - q_t)^2 \quad (5)$$

where k_2 is the adsorption rate constant of the pseudo-second order model (g/mmol min).

Gibbs free energy (ΔG), standard enthalpy (ΔH) and entropy (ΔS) were calculated from adsorption isotherms at various temperatures. The thermodynamic characteristics were calculated analytically using the equations [42]:

$$\Delta G^0 = -RT \ln K_c \quad (6)$$

where K_c is the thermodynamic equilibrium constant, which can be determined from the equation:

$$K_c = \frac{C_t}{C_e} \quad (7)$$

The Gibbs equation can also be expressed as follows:

$$\Delta G^0 = \Delta H^0 - T\Delta S^0 \quad (8)$$

2.4.3. Study of the Dependence of Sorption on the pH

Dye solutions with a volume of 40 mL and a concentration of 20 mg/L were placed in a 100 mL beaker and thermostated at 278, 293 and 308 K on a magnetic stirrer. The pH of the initial solution was adjusted by adding 0.1 N NaOH or HCl solution dropwise. Next, adsorption studies were conducted, as mentioned earlier.

2.4.4. Determining the Number of Work Cycles

A certain volume of a dye solution with a standard concentration is placed in a beaker and thermostated at a given temperature. The calculated mass of the sorbent is added and kept at a given temperature until the equivalence point is reached (at least 3 h). The sorbent is separated by centrifugation, washed with cold distilled water and treated with an eluent (ethanol) at a temperature of 40–50 °C to desorb the dye; the procedure is repeated several times until the color of the eluent is gone. The sorbent is washed repeatedly with water and conditioned. The procedure is repeated 4–5 times.

3. Results

3.1. Synthesis and Characterization of the Sorbent

In this work, we considered the removal of dyes from an aqueous medium using a MOF-GO nanocomposite material obtained by the in situ method. A characteristic feature of this synthesis is the introduction of GO at the stage of MOF synthesis to generate MOF crystals on the surface of GO with a size of up to 100 nm, which leads to the formation of a nanocomposite material.

The initial GO sample was analyzed by elemental analysis, using EDX analysis and conventional combustion to determine the content of the elements. Found (%): C–66.5; O–31.8 (EDX analysis, Figure 2); C–66.4; H–1.72 (burning method).

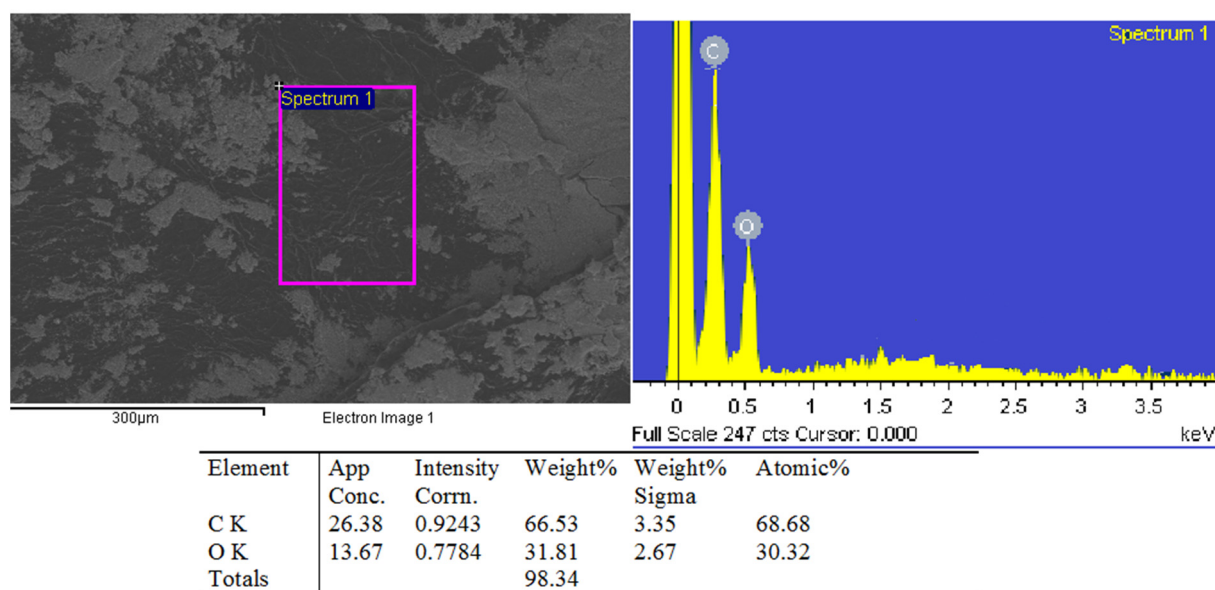


Figure 2. Photomicrograph of a section of the surface of a GO sheet and elemental analysis at this point.

We have obtained the IR spectra of the key compounds involved in the synthesis of the composite by pressing in a tablet with potassium bromide in the frequency range from 4000 to 400 cm^{-1} (Figure 3). The IR spectrum of GO (Figure 3a) contains a peak in the region of 3400 cm^{-1} , assignable to stretching vibrations of hydroxy groups of adsorbed water. There are absorption bands in the region of 2927 and 2849 cm^{-1} , characteristic of symmetric and asymmetric vibrations of CH_2 groups, an intense band in the region of 1720 cm^{-1} , corresponding to vibrations of the carboxyl group, and a low-intensity band in the region of 1619 cm^{-1} , corresponding to vibrations of C-C bonds which are probably due to a slight admixture of unoxidized graphite [43]. These data agree well with the results of studying laboratory and commercial samples of graphene oxide [44,45]. In the IR spectrum of copper trimesinate (Figure 3c), one can see the formation of a strong absorption peak in the region of 760 cm^{-1} , which can be interpreted as the formation of a Me-O bond. This proves that deprotonation of carboxyl groups occurred with the formation of a Cu-O bond.

However, in the composite, such a peak is shifted by 20 cm^{-1} to the long wavelength region. Characteristically, in copper trimesinate, the intense band of pure trimesic acid in the region of 1720 cm^{-1} , corresponding to the carboxyl group in the non-ionized form, completely disappears. This allows us to assert that there are no free carboxyl groups in the obtained complex; all three carboxyl groups are deprotonated and form bonds with copper atoms. In the IR spectrum of copper trimesinate, new bands appear at 1375 and 1560 cm^{-1} , which are characteristic of symmetric and asymmetric vibrations of carboxy groups. Since $\Delta\nu = 185\text{ cm}^{-1}$, it can be argued that the carboxylate ion can exhibit the character of both a monodentate and a bidentate ligand. In the composite, these peaks are preserved. At the same time, GO introduces into the composite a wide strong band with a peak in the region of 3400 cm^{-1} , which can be attributed to stretching vibrations of adsorbed water hydroxo groups. The intense band at 1740 cm^{-1} corresponds to vibrations of carboxyl groups and epoxy carbon atoms, which are also contributed by GO. The absorption band at 1625 cm^{-1} refers to bending vibrations of hydroxo groups. Intense absorption bands at 1200 , 1100 and 850 cm^{-1} can also characterize the formation of epoxy groups. The IR spectrum of the resulting composite includes a set of spectra of GO and copper trimesinate, regardless of the amount of GO (Figure 3d).

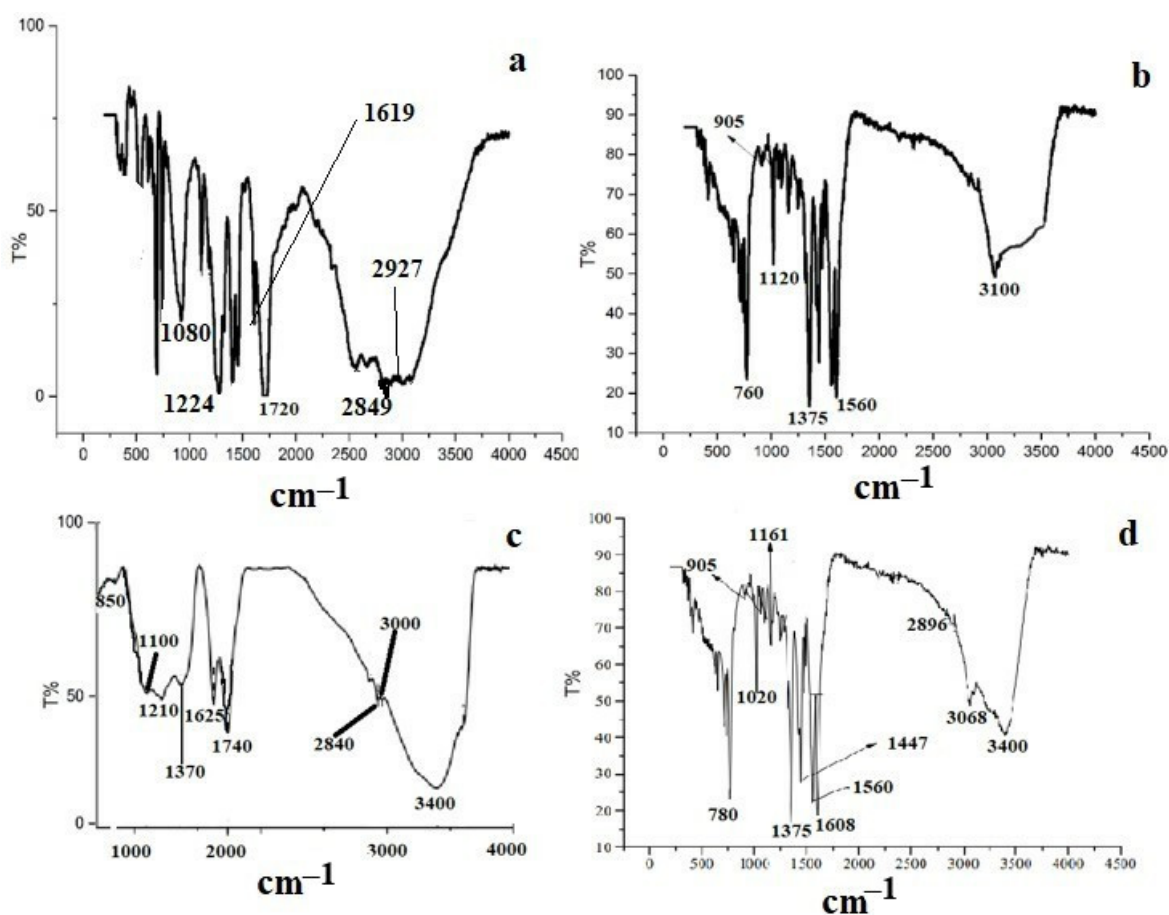


Figure 3. IR spectra of GO (a), copper trimesinate (b), trimesic acid (c) and nanocomposite (d).

Since porosity is an important parameter of porous materials as dye adsorbents, the specific surface area, total pore volume and pore size distribution of MOF and MOF-GO composites were analyzed using N_2 adsorption-desorption isotherms at 77 K. All samples show typical type I isotherms according to the IUPAC classification, suggesting the predominance of micropores existing in the materials. A high ratio of micropore volume to total pore volume ($V_{\text{micro}}/V_{\text{total}}$) above 70% can also confirm this. As can be seen from Table 2, MOF has a large surface area of $1562\text{ m}^2/\text{g}$ and a pore volume of $0.85\text{ cm}^3/\text{g}$. GO

is not porous when nitrogen is used as a molecular probe [46], and a low content of GO in composites leads to a slight decrease in the surface area of MOFs [31]. In our work, a significant increase in the GO content leads to a sharp decrease in the surface area and the average pore radius in all three composites due to the structure of the coating. At the same time, V_{total} and V_{micro} practically do not change, which indicates the same microporous nature of MOFs and composites.

Table 2. Characteristics of MOFs, GO and nanocomposites.

Sample	S_{BET} (m^2/g)	V_{total} (cm^3/g)	V_{micro} (cm^3/g)	Average Pore Radius (\AA)
MOF	1562.3	0.85	0.61	10.9
GO	562	-	-	6.2
Nanocomposite (5% GO)	762	0.85	0.6	6.5
Nanocomposite (10% GO)	713	0.85	0.6	6.6
Nanocomposite (20% GO)	689	0.85	0.6	6.8

The composite does not form as dense of a structure as the initial MOF does, but it has a layered structure irrespective of the amount of the introduced GO (Figure 4). GO sheets are directly adjacent to copper trimesinate crystals, forming a common system. The diffraction patterns of the composites have a similar shape which does not depend on the GO content and coincides with the previously published data [47].

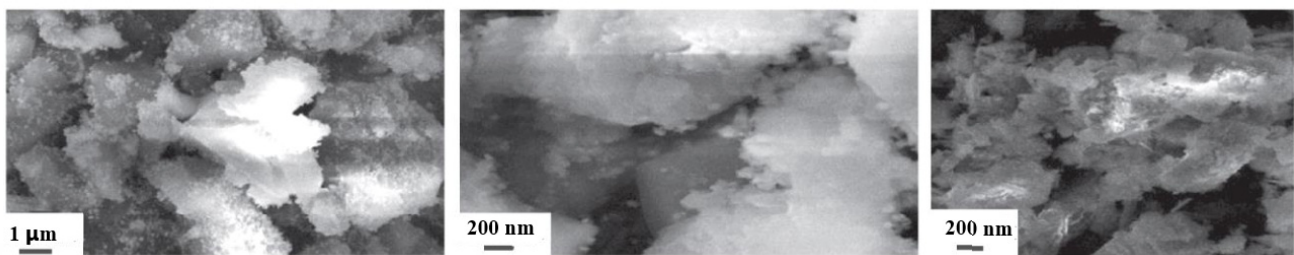


Figure 4. SEM images of the composites of copper trimesinate with 5, 10 and 20% GO, respectively.

Based on the data we obtained and the available literature data, the following structure can be assigned to the composites (Figure 5).

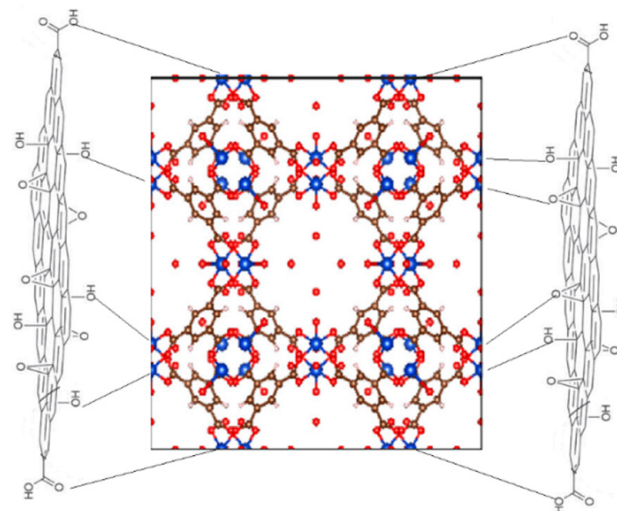


Figure 5. Scheme of the location of copper trimesinate between graphene layers in the composite. The Cu atoms are shown in blue; O atoms, red; C atoms, brown; H atoms, pink.

3.2. Adsorption of Dyes on the Sorbent

The adsorption isotherm plays a crucial role in analyzing the adsorption capacity of the materials and providing information about the solution–surface interaction. The adsorption capacity of the sorbent with the increase in the initial dye concentration is shown in Figure 6. The adsorbed amounts of the dyes increased with the increase in equilibrium dye concentration. It is evident that a high concentration in the solution implicates a high dye molecule fixed at the surface of the adsorbent. When studying the dependence of the solid-phase extraction on the initial concentration, it is noticeable that, with an increase in the initial concentration of the sorbate, the adsorption increases monotonically.

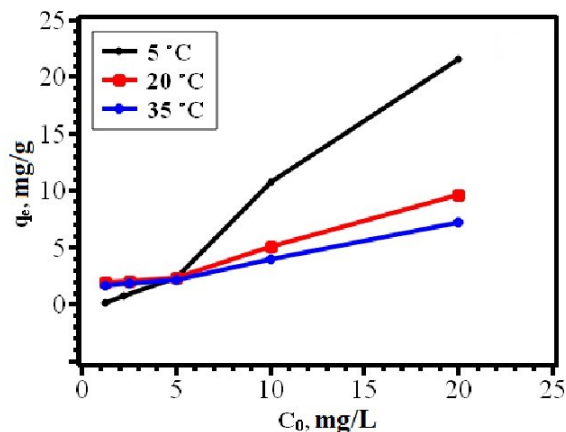


Figure 6. Dependence of the extraction on the initial concentration of the sorbate for IC dye.

An analysis of the parameters of the Langmuir adsorption isotherm model (Figure 7) allows us to conclude that this Langmuir model describes the adsorption process well. The correlation coefficients are quite high, and the maximum adsorption calculated by the Langmuir model satisfactorily coincides with the experimental one (Table 3).

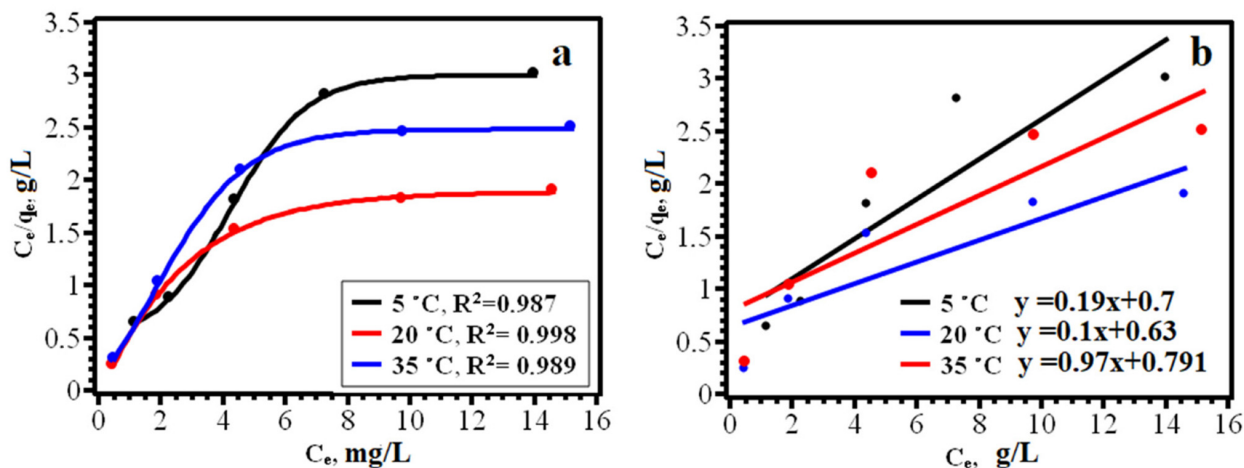


Figure 7. Langmuir isotherms of the solid-phase extraction of IC dye in non-linearized (a) and linearized (b) form.

An analysis of the Freundlich adsorption isotherms shows that the obtained experimental data satisfactorily agree with this model, since the correlation coefficient is quite high (R^2 is more than 0.91) (Figure 8). The values of the Freundlich constants within the framework of the description of this model characterize the resulting composites as sorbents with satisfactory adsorption properties. The values of the coefficient $1/n$ range from 0 to 1, which indicates favorable conditions for adsorption and is in good agreement with the other experimental data (Table 3).

Table 3. Isotherm model constants of dyes by the nanocomposite.

Model	Sorbate	Constants	T (K)		
			283	293	308
<i>Nanocomposite with 5% GO</i>					
Langmuir	CV	q_{max} (mg/g)	90.9	74.3	53.1
		K_L (L/mg)	0.036	0.013	0.010
		R^2	0.992	0.980	0.883
	RB	q_{max} (mg/g)	29.0	21.4	19.6
		K_L (L/mg)	3.31	2.20	2.02
		R^2	0.959	0.765	0.855
	MG	q_{max} (mg/g)	37.00	29.4	18.8
		K_L (L/mg)	0.03	0.11	0.53
		R^2	0.890	0.983	0.964
	BG	q_{max} (mg/g)	35.5	29.2	27.1
		K_L (L/mg)	1.29	1.11	0.76
		R^2	0.938	0.949	0.918
	IC	q_{max} (mg/g)	27.6	17.5	12.4
		K_L (L/mg)	0.78	0.66	0.60
		R^2	0.814	0.756	0.737
Freundlich	CV	$1/n$	0.997	0.73	0.63
		K_F ($mg^{1-1/n}/g \cdot L^{-1/n}$)	0.11	0.32	0.35
		R^2	0.951	0.913	0.965
	RB	$1/n$	0.71	0.75	0.78
		K_F ($mg^{1-1/n}/g \cdot L^{-1/n}$)	0.10	0.07	0.08
		R^2	0.972	0.969	0.966
	MG	$1/n$	0.53	0.64	0.60
		K_F ($mg^{1-1/n}/g \cdot L^{-1/n}$)	0.85	0.20	0.10
		R^2	0.945	0.960	0.930
	BG	$1/n$	0.84	0.65	0.58
		K_F ($mg^{1-1/n}/g \cdot L^{-1/n}$)	0.16	0.22	0.24
		R^2	0.956	0.939	0.998
	IC	$1/n$	0.90	0.53	0.32
		K_F ($mg^{1-1/n}/g \cdot L^{-1/n}$)	0.10	0.20	0.40
		R^2	0.911	0.979	0.919
<i>Nanocomposite with 10% GO</i>					
Langmuir	CV	q_{max} (mg/g)	27.27	22.46	21.45
		K_L (L/mg)	0.13	0.18	0.17
		R^2	0.806	0.795	0.768
	RB	q_{max} (mg/g)	34.88	32.41	30.54
		K_L (L/mg)	0.13	0.14	0.12
		R^2	0.973	0.934	0.924
	MG	q_{max} (mg/g)	9.03	8.67	8.01
		K_L (L/mg)	0.19	0.18	0.17
		R^2	0.876	0.847	0.879
	BG	q_{max} (mg/g)	32.71	29.04	20.50
		K_L (L/mg)	0.06	0.05	0.07
		R^2	0.942	0.917	0.913
	IC	q_{max} (mg/g)	18.05	15.40	15.10
		K_L (L/mg)	0.04	0.02	0.015
		R^2	0.869	0.910	0.923

Table 3. Cont.

Model	Sorbate	Constants	T (K)		
			283	293	308
Freundlich	CV	1/n	0.60	0.62	0.63
		$K_F (mg^{1-1/n}/g \cdot L^{-1/n})$	2.51	2.46	2.34
		R^2	0.990	0.991	0.989
	RB	1/n	0.58	0.55	0.53
		$K_F (mg^{1-1/n}/g \cdot L^{-1/n})$	1.16	1.12	1.08
		R^2	0.844	0.797	0.776
	MG	1/n	0.55	0.54	0.53
		$K_F (mg^{1-1/n}/g \cdot L^{-1/n})$	1.99	1.79	1.67
		R^2	0.936	0.939	0.940
	BG	1/n	0.69	0.65	0.60
$K_F (mg^{1-1/n}/g \cdot L^{-1/n})$		1.27	1.13	1.04	
R^2		0.961	0.939	0.910	
IC	1/n	0.61	0.51	0.49	
	$K_F (mg^{1-1/n}/g \cdot L^{-1/n})$	1.85	1.35	1.08	
	R^2	0.981	0.994	0.998	
<i>Nanocomposite with 20% GO</i>					
Langmuir	CV	$q_{max} (mg/g)$	30.77	24.75	23.56
		$K_L (L/mg)$	0.18	0.21	0.14
		R^2	0.998	0.957	0.967
	RB	$q_{max} (mg/g)$	30.78	21.44	18.04
		$K_L (L/mg)$	0.21	0.28	0.32
		R^2	0.922	0.823	0.851
	MG	$q_{max} (mg/g)$	24.75	16.00	13.76
		$K_L (L/mg)$	0.06	0.17	0.20
		R^2	0.945	0.946	0.961
	BG	$q_{max} (mg/g)$	27.47	18.81	16.64
$K_L (L/mg)$		0.13	0.16	0.17	
R^2		0.977	0.953	0.975	
IC	$q_{max} (mg/g)$	14.88	13.04	12.05	
	$K_L (L/mg)$	0.12	0.11	0.10	
	R^2	0.819	0.886	0.970	
Freundlich	CV	1/n	0.75	0.70	0.69
		$K_F (mg^{1-1/n}/g \cdot L^{-1/n})$	3.142	3.050	2.268
		R^2	0.984	0.993	0.985
	RB	1/n	0.53	0.55	0.56
		$K_F (mg^{1-1/n}/g \cdot L^{-1/n})$	3.370	2.838	2.532
		R^2	0.998	0.996	0.994
	MG	1/n	0.81	0.80	0.82
		$K_F (mg^{1-1/n}/g \cdot L^{-1/n})$	1.390	1.333	1.290
		R^2	0.999	0.998	0.999
	BG	1/n	0.73	0.60	0.58
$K_F (mg^{1-1/n}/g \cdot L^{-1/n})$		3.005	2.950	2.803	
R^2		0.947	0.979	0.973	
IC	1/n	0.55	0.60	0.75	
	$K_F (mg^{1-1/n}/g \cdot L^{-1/n})$	1.853	1.501	1.030	
	R^2	0.984	0.996	0.992	

Contact time is an important design parameter on which the adsorption process depends, as it provides information about the dynamic of the reaction in terms of the

order and the rate constant. As shown in Figure 9, the degree of extraction of dyes on the composite increases rapidly during the initial contact time and then slows down. Rapid diffusion to the outer surface is accompanied by diffusion into the pores of the matrix at a significant rate, which ultimately leads to a rapid achievement of equilibrium.

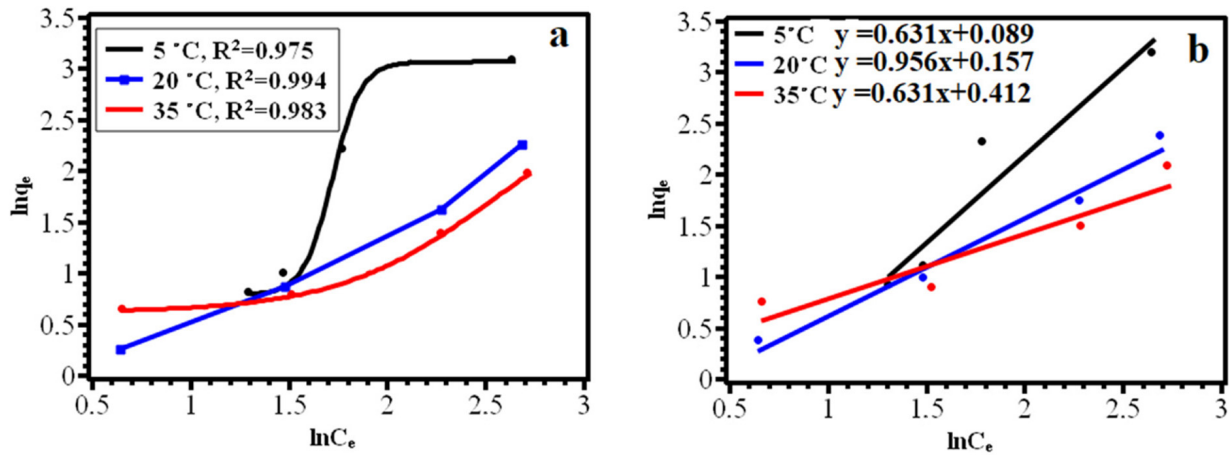


Figure 8. Freundlich isotherms of the solid-phase extraction of IC dye in non-linearized (a) and linearized (b) form.

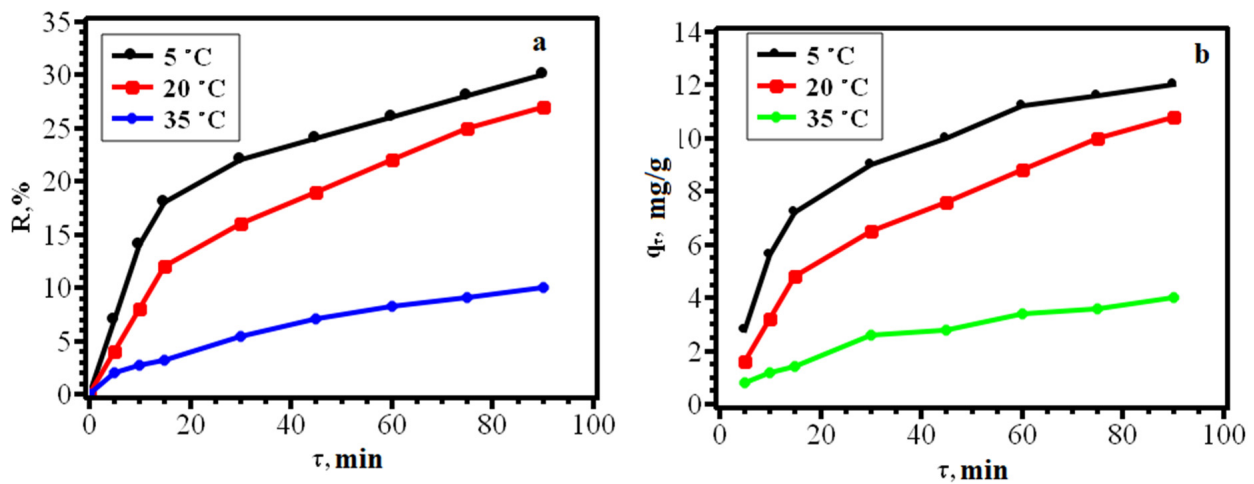


Figure 9. Degree of extraction (a) and kinetic curves (b) of solid-phase extraction versus contact time for IC dye.

The linear plots of $\ln(q_e - q_t)$ versus t for a pseudo-first order reaction and of t/q_t versus t for a pseudo-second order reaction for dye adsorption were evaluated to obtain the rate parameters. Kinetic parameters under different conditions were calculated from the graphs (Figure 10). The applied pseudo-first-order equation satisfactorily describes the patterns of adsorption at the initial stages (up to 60 min in the experiment) of the adsorption process, when the phenomenon of film diffusion has a significant effect on the process. Apparently, an increase in the concentration of sorbate molecules at the surface of the adsorbent at the initial moments of the process and at low degrees of the filling of the adsorption space stimulates the movement of sorbate molecules into the pores of the adsorbent under the influence of the concentration gradient, but, subsequently, this process slows down, which in turn potentiates other mechanisms. The calculated values of the determination coefficient make it possible to judge that the pseudo-first-order kinetic adsorption model describes the process less accurately, and, consequently, the pseudo-second-order kinetic model is more preferable (Table 4).

Table 4. Kinetic parameters of the process of adsorption by a nanocomposite.

Dye	T (K)	C_e (mg/g)	Time to Reach Equilibrium (min)	R^2		k_1 (min ⁻¹)	$k_2 \times 10^{-3}$ (g/mg min)
				Pseudo-First Order	Pseudo-Second Order		
<i>Nanocomposite with 5% GO</i>							
IC	278	14.05	90	0.950	0.990	0.60	0.36
	293	14.63	90	0.985	0.982	0.65	0.34
	308	18.01	90	0.955	0.951	0.81	1.66
BG	278	8.88	90	0.988	0.988	0.68	2.03
	293	9.56	90	0.982	0.972	0.81	1.59
	308	11.28	90	0.990	0.938	0.55	1.45
CV	278	6.64	90	0.987	0.995	0.68	1.19
	293	7.94	90	0.976	0.998	0.60	1.52
	308	9.86	90	0.960	0.962	0.65	1.76
RB	278	5.10	90	0.966	0.889	0.61	1.02
	293	5.18	90	0.974	0.895	0.51	0.98
	308	5.65	90	0.996	0.995	0.34	0.86
MG	278	14.50	90	0.923	0.963	0.45	2.24
	293	15.38	90	0.996	0.998	0.60	5.69
	308	17.94	90	0.958	0.994	0.62	19.61
<i>Nanocomposite with 10% GO</i>							
IC	278	14.88	90	0.952	0.955	0.55	1.35
	293	16.10	90	0.980	0.925	0.73	1.26
	308	16.54	90	0.901	0.972	1.11	13.40
BG	278	10.36	90	0.995	0.922	0.40	1.33
	293	10.96	90	0.994	0.976	0.55	1.65
	308	11.16	90	0.988	0.946	0.65	1.94
CV	278	6.30	90	0.990	0.941	0.67	0.77
	293	6.57	90	0.988	0.929	0.70	0.76
	308	6.72	90	0.986	0.948	0.73	0.75
RB	278	4.76	90	0.938	0.995	0.60	2.80
	293	5.08	90	0.951	0.996	0.61	2.77
	308	5.20	90	0.957	0.992	0.63	2.74
MG	278	15.54	90	0.992	0.968	0.60	3.81
	293	15.90	90	0.961	0.977	0.93	5.58
	308	16.70	90	0.977	0.917	0.41	4.55
<i>Nanocomposite with 20% GO</i>							
IC	278	12.92	90	0.955	0.928	0.65	1.18
	293	12.98	90	0.936	0.967	0.61	1.05
	308	13.04	90	0.938	0.972	0.51	1.01
BG	278	8.80	90	0.964	0.964	0.73	1.49
	293	10.26	90	0.900	0.975	0.60	1.70
	308	12.00	90	0.951	0.855	0.70	1.10
CV	278	6.00	90	0.953	0.953	0.63	0.69
	293	6.70	90	0.938	0.955	0.68	0.76
	308	7.70	90	0.924	0.962	0.70	0.82
RB	278	4.42	90	0.988	0.963	0.87	0.80
	293	4.70	90	0.978	0.977	0.61	0.71
	308	4.95	90	0.967	0.984	0.53	0.65
MG	278	10.50	90	0.850	0.950	0.31	1.23
	293	10.70	90	0.873	0.971	0.35	1.25
	308	11.20	90	0.965	0.889	0.47	1.36

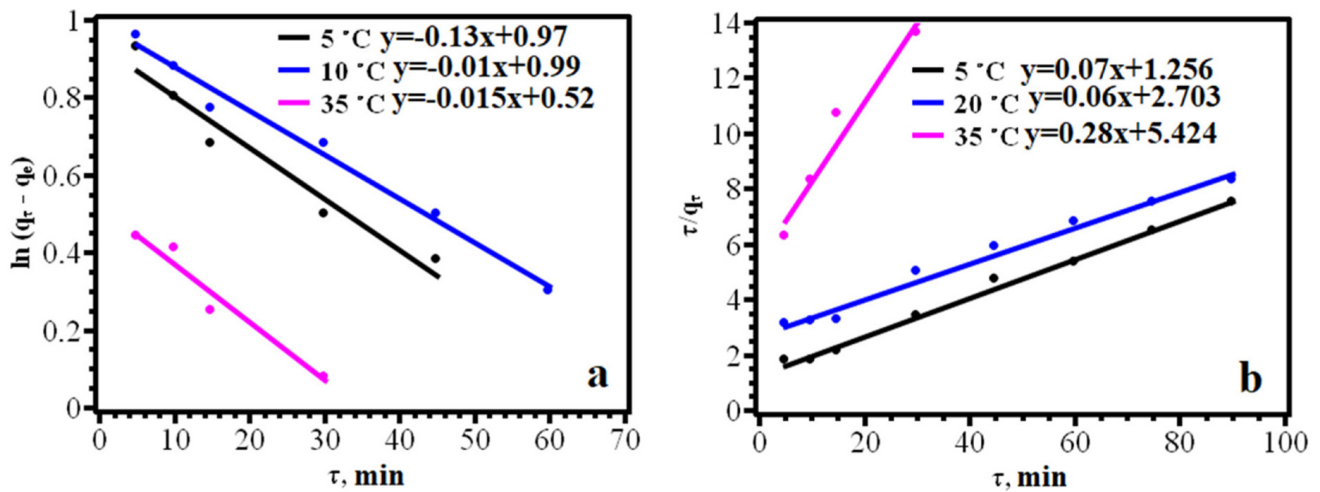


Figure 10. Pseudo-first order (a) and pseudo-second order (b) models of the solid-phase extraction rate for IC dye.

From the data given in Table 5, we can conclude that positive adsorption enthalpies characterize the process as endothermic, except for the processes of solid-phase extraction with a nanocomposite containing 5% GO of the dyes MG and IR. For these dyes, the enthalpy value has negative values, which characterize the processes as exothermic. In order for the organic dye particles to reach the active centers of the adsorbent, it is necessary that they be freed from the hydration shell, or at least part of it, for which energy must be expended. As a result, the calculated value of the enthalpy is the result of two processes—the dehydration of organic dye ions (an endothermic process) and the adsorption of the latter on the active centers of the adsorbent, which proceeds with the release of energy (the heat of adsorption). A positive entropy value indicates an increase in the number of degrees of freedom at the solid–liquid interface during the dye adsorption process and reflects the sorbate affinity for adsorbent molecules. The activation energies are small values, which indicate the feasibility of the adsorption process under these conditions. In addition, since the values are below 40 kJ/mol, it can be assumed with a reasonable degree of confidence that the limiting process is physical adsorption.

Table 5. Thermodynamic parameters of dye adsorption by the nanocomposite.

Sorbate	T, K	K_c	ΔG^0 (kJ/mol)	ΔH^0 (kJ/mol)	ΔS^0 (J/mol K)
<i>Nanocomposite with 5% GO</i>					
CV	278	1.420	−2.513	0.12	12.1
	293	1.512	−2.189		
	308	1.705	−2.103		
RB	278	1.592	−4.089	0.67	1.57
	293	1.680	−4.203		
	308	1.769	−4.115		
MG	278	1.873	−5.835	−0.93	1.86
	293	2.315	−6.112		
	308	2.562	−4.768		
BG	278	0.425	−2.123	0.84	0.42
	293	0.769	−1.912		
	308	0.913	−1.105		
IC	278	2.440	−5.636	−1.28	10.6
	293	2.211	−5.356		
	308	0.280	−0.7		

Table 5. Cont.

Sorbate	T, K	K _c	ΔG ⁰ (kJ/mol)	ΔH ⁰ (kJ/mol)	ΔS ⁰ (J/mol K)
<i>Nanocomposite with 10% GO</i>					
CV	278	1.470	−3.398	0.810	8.94
	293	1.408	−3.430		
	308	1.374	−3.518		
RB	278	1.857	−4.292	0.727	12.24
	293	1.771	−4.314		
	308	1.739	−4.453		
MG	278	1.928	−4.456	0.715	8.11
	293	1.662	−4.049		
	308	1.555	−3.982		
BG	278	0.621	−1.435	0.694	6.53
	293	0.501	−1.220		
	308	0.460	−1.178		
IC	278	1.071	−2.476	0.702	6.74
	293	0.510	−1.242		
	308	0.374	−0.958		
<i>Nanocomposite with 20% GO</i>					
CV	278	1.541	−3.562	0.732	8.98
	293	1.379	−3.359		
	308	1.162	−2.976		
RB	278	1.953	−4.514	0.577	17.53
	293	1.873	−4.560		
	308	1.805	−4.622		
MG	278	1.717	−3.968	0.725	16.09
	293	1.638	−3.990		
	308	1.571	−4.023		
BG	278	0.934	−2.159	0.754	7.90
	293	0.641	−1.561		
	308	0.289	−0.740		
IC	278	0.092	−0.213	0.781	2.01
	293	0.079	−0.192		
	308	0.065	−0.166		

The study of the dependence of solid-phase extraction on the pH of the medium allows us to conclude that the obtained sorbent can be used for extraction in a wide pH range, illustrating the excellent pH window offered by this adsorbent (Table 6).

Table 6. Dependence of the degree of extraction of the dyes by the composite (5% GO) on the pH.

BG	pH	2	3	4	5	6	7	8		
	R (%)	51.7	51.9	51.9	51.9	52	52.2	52.2		
CV	pH	2	3	4	5	6	7	8	9	10
	R (%)	48.3	50.4	57.2	60.3	60.3	60.3	50.7	43.2	30.1
RB	pH			4	5	6	7	8	9	10
	R (%)	60.3	68.2	74.1	74.1	74.1	74.1	74.0	73.8	73.6
MG	pH			4	5	6	7	8	9	10
	R (%)			23	23	23.1	23.1	23.1	23.1	23.1
IC	pH			4	5	6	7	8	9	10
	R (%)			25	25.3	25.4	25.6	25.6	25.5	24

The possibility of the repeated use of the sorbent for the extraction of dyes is an important parameter. Studies have been conducted on the regeneration of the sorbent after use in the adsorption of dyes. The data obtained (Table 7) show that the sorbent can be used for five cycles without a significant loss of sorption capacity.

Table 7. Dependence of the degree of extraction on the number of working cycles.

CV	Cycle	1	2	3	4	5
5% GO	R, %	60.3	55.7	51.1	46.2	39.4
CV	Cycle	1	2	3	4	5
10% GO	R, %	67.6	67.4	67.1	66.4	65.2
CV	Cycle	1	2	3	4	5
20% GO	R, %	76.5	76.1	75.8	75.2	73.1
BG	Cycle	1	2	3	4	5
5% GO	R, %	52.2	48.6	44.2	38.7	32.1
BG	Cycle	1	2	3	4	5
10% GO	R, %	45.4	45.2	44.6	40.1	38.7
BG	Cycle	1	2	3	4	5
20% GO	R, %	42.7	42.1	41.5	40.1	38.6
RB	Cycle	1	2	3	4	5
5% GO	R, %	74.2	72.3	70.4	68.1	60.2
RB	Cycle	1	2	3	4	5
10% GO	R, %	74.7	74.2	73.8	78.2	72.6
RB	Cycle	1	2	3	4	5
20% GO	R, %	76.6	76.1	75.4	70.3	68.6
MG	Cycle	1	2	3	4	5
5% GO	R, %	23.1	22.4	21.6	20.1	18.1
MG	Cycle	1	2	3	4	5
10% GO	R, %	20.6	20.5	20.3	20.1	19.8
MG	Cycle	1	2	3	4	5
20% GO	R, %	46.6	46.2	45.2	41.4	38.2
IC	Cycle	1	2	3	4	5
5% GO	R, %	25.7	25.6	25.5	25.3	25.1
IC	Cycle	1	2	3	4	5
10% GO	Cycle	35.2	35.0	34.8	34.1	33.3

The sorbent makes it possible to achieve a maximum sorption of 393 mg/g, which is a sufficiently high value for the absorption of dyes (Table 8). The complex is an effective sorbent for the extraction of cationic and neutral organic dyes when the content of GO in the nanocomposite is 20 wt.% of the calculated copper trimesinate. With an increase in the content of GO, which consists of many carboxyl groups, in the composite in addition to physical sorption on the composite, cationic and neutral dyes are also bound chemically on GO. In the case of anionic dyes, the maximum adsorption is achieved when using a composite containing 5% GO due to the predominance of physical sorption. A comparison of the maximum adsorption values for the studied dyes leads to the conclusion that cationic dyes are adsorbed best. From the obtained metrological characteristics of the adsorption of dyes, presented in Table 8, we can conclude that the accuracy score does not exceed 4%, and the accuracy rate does not exceed 5%.

Table 8. Values of maximum adsorption and degree of extraction for studied dyes ($n = 3, p = 0.95$).

Dye	GO Content in the Composite (%)	Dye Nature	q_{\max} (mg/g)	R (%)	Limit of Detection (mg/L)	Limit of Quantification (mg/L)	Accuracy Score (Systematic Error) $\pm \Delta c$ (%)	Accuracy Rate (Error Characteristic) $\pm \Delta$ (%)
IC	5%	Anionic	196.0	25.6	0.625	0.625–10	$3.1 \pm 2\%$	$4.2 \pm 2\%$
	10%	Anionic	105.6	35.4	0.3	0.3–12.4	$3.1 \pm 2\%$	$4.2 \pm 2\%$
	20%	Anionic	187.5	35.4	0.625	0.625–7.5	$3.1 \pm 2\%$	$4.2 \pm 2\%$
BG	5%	Cationic	74.8	55.6	0.3	0.3–20	$3.4 \pm 3\%$	$3.7 \pm 3\%$
	10%	Cationic	128	48.2	0.3	0.3–20	$3.4 \pm 3\%$	$3.7 \pm 3\%$
	20%	Cationic	130	56.0	0.3	0.3–20	$3.4 \pm 3\%$	$3.7 \pm 3\%$
MG	5%	Cationic	89.3	27.5	0.625	0.625–15.2	$5.1 \pm 2\%$	$2.9 \pm 2\%$
	10%	Cationic	51.5	22.3	1.25	1.25–20	$5.1 \pm 2\%$	$2.9 \pm 2\%$
	20%	Cationic	233.6	47.5	0.625	0.625–20	$5.1 \pm 2\%$	$2.9 \pm 2\%$
RB	5%	Neutral	84.0	74.5	0.3	0.3–20	$2.9 \pm 4\%$	$2.1 \pm 3\%$
	10%	Neutral	304.0	76.2	0.3	0.3–20	$2.9 \pm 4\%$	$2.1 \pm 3\%$
	20%	Neutral	345.6	77.9	0.3	0.3–20	$2.9 \pm 4\%$	$2.1 \pm 3\%$
CV	5%	Cationic	93.0	68.5	0.3	0.3–20	$3.7 \pm 2\%$	$3.5 \pm 2\%$
	10%	Cationic	380.4	68.5	0.3	0.3–20	$3.7 \pm 2\%$	$3.5 \pm 2\%$
	20%	Cationic	393.0	70.0	0.3	0.3–20	$3.7 \pm 2\%$	$3.5 \pm 2\%$

4. Conclusions

The developed one-stage method for the in situ preparation of composites based on a copper trimesinate and graphene oxide is economical and can be used for large-scale production. The IR spectrum of the resulting composite includes a set of spectra of graphene oxide and copper trimesinate, regardless of the amount of graphene oxide. The diffraction patterns of the composites have similar shapes, which do not also depend on the graphene oxide content. Nanocomposites showed a good ability to adsorb organic dyes, such as malachite green, indigo carmine, brilliant green, Rose Bengal and crystal violet. The complex is an effective sorbent for the extraction of cationic and neutral organic dyes when the content of GO in the nanocomposite is 20 wt.% of the calculated copper trimesinate. In the case of anionic dyes, the maximum adsorption is achieved when using a composite containing 5% GO. The accuracy score does not exceed 4%, and the accuracy rate does not exceed 5%. The sorbent can be used for five cycles without a significant loss of sorption capacity.

Author Contributions: Conceptualization, I.E.U. and V.A.Z.; methodology, I.E.U., V.N.N. and V.A.Z.; writing—original draft, I.E.U. and V.A.Z.; writing—review and editing, I.E.U., V.N.N. and V.A.Z.; supervision, I.E.U. All authors have read and agreed to the published version of the manuscript.

Funding: This research received no external funding.

Institutional Review Board Statement: Not applicable.

Informed Consent Statement: Not applicable.

Data Availability Statement: The data presented in this study are available in the article.

Conflicts of Interest: The authors declare no conflict of interest.

References

- Abe, F.R.; Mendonça, J.N.; Moraes, L.A.; de Oliveira, G.A.; Gravato, C.; Soares, A.M.; de Oliveira, D.P. Toxicological and behavioral responses as a tool to assess the effects of natural and synthetic dyes on zebrafish early life. *Chemosphere* **2017**, *178*, 282–290. [[CrossRef](#)] [[PubMed](#)]
- Li, J.; Wang, L.; Liu, Y.; Song, Y.; Zeng, P.; Zhang, Y. The research trends of metal-organic frameworks in environmental science: A review based on bibliometric analysis. *Environ. Sci. Pollut. Res.* **2020**, *27*, 19265–19284. [[CrossRef](#)] [[PubMed](#)]

3. Pavithra, K.G.; Kumar, P.S.; Jaikumar, V.; Rajan, P.S. Removal of colorants from wastewater: A review on sources and treatment strategies. *J. Ind. Eng. Chem.* **2019**, *75*, 1–19. [[CrossRef](#)]
4. Gorbunova, M.O.; Bayan, E.M.; Shevchenko, A.V.; Kulyaginova, M.S. Digital colorimetric determination of chlorides in water using gas extraction and methyl orange. *Anal. Kontrol* **2017**, *21*, 274–280. [[CrossRef](#)]
5. Khan, M.A.; Khan, M.I.; Zafar, S. Removal of different anionic dyes from aqueous solution by anion exchange membrane. *Membr. Water Treat.* **2017**, *8*, 259–277. [[CrossRef](#)]
6. Zwane, S.; Masheane, M.L.; Kuvarega, A.T.; Vilakati, G.D.; Mamba, B.B.; Nyoni, H.; Mhlanga, S.D.; Dlamini, D.S. Polyethersulfone/Chromolaena odorata (PES/CO) adsorptive membranes for removal of Congo red from water. *J. Water Process. Eng.* **2019**, *30*, 100498. [[CrossRef](#)]
7. Xiao, X.Z.; Dai, T.T.; Guo, J.; Wu, J.H. Flowerlike Brochantite Nanoplate Superstructures for Catalytic Wet Peroxide Oxidation of Congo Red. *ACS Appl. Nano Mater.* **2019**, *2*, 4159–4168. [[CrossRef](#)]
8. Khan, J.; Sayed, M.; Ali, F.; Khan, H.M. Removal of Acid Yellow 17 Dye by Fenton Oxidation Process. *Z. Phys. Chem.* **2018**, *232*, 507–525. [[CrossRef](#)]
9. Rashed, M.N.; Eltaher, M.A.; Abdou, A.N.A. Adsorption and photocatalysis for methyl orange and Cd removal from wastewater using TiO₂/sewage sludge-based activated carbon nanocomposites. *R. Soc. Open Sci.* **2017**, *4*, 170834. [[CrossRef](#)]
10. Xu, R.; Su, M.; Liu, Y.; Chen, Z.; Ji, C.; Yang, M.; Chang, X.; Chen, D. Comparative study on the removal of different-type organic pollutants on hierarchical tetragonal bismutite microspheres: Adsorption, degradation and mechanism. *J. Clean. Prod.* **2020**, *242*, 118366. [[CrossRef](#)]
11. Tran, V.A.; Vu, K.B.; Vo, T.-T.; Le, V.T.; Do, H.H.; Bach, L.G.; Lee, S.-W. Experimental and computational investigation on interaction mechanism of Rhodamine B adsorption and photodegradation by zeolite imidazole frameworks-8. *Appl. Surf. Sci.* **2021**, *538*, 148065. [[CrossRef](#)]
12. Abdellah, M.H.; Nosier, S.A.; El-Shazly, A.H.; Mubarak, A.A. Photocatalytic decolorization of methylene blue using TiO₂/UV system enhanced by air sparging. *Alex. Eng. J.* **2018**, *57*, 3727. [[CrossRef](#)]
13. Garcia-Segura, S.; Ocon, J.D.; Chong, M.N. Electrochemical oxidation remediation of real wastewater effluents—A review. *Process Saf. Environ.* **2018**, *113*, 48–67. [[CrossRef](#)]
14. Pacheco-Alvarez, M.O.A.; Picos, A.; Perez-Segura, T.; Peralta-Hernandez, J.M. Proposal for highly efficient electrochemical discoloration and degradation of azo dyes with parallel arrangement electrodes. *J. Electroanal. Chem.* **2019**, *838*, 195–203. [[CrossRef](#)]
15. Goma, O.M.; Fapetu, S.; Kyazze, G.; Keshavarz, T. Probing the mechanism of simultaneous bioenergy production and biodegradation process of Congo red in microbial fuel cells. *J. Chem. Technol. Biotechnol.* **2019**, *94*, 2092–2097. [[CrossRef](#)]
16. Shanmugam, S.; Ulaganathan, P.; Swaminathan, K.; Sadhasivam, S.; Wu, Y.R. Enhanced biodegradation and detoxification of malachite green by *Trichoderma asperellum* laccase: Degradation pathway and product analysis. *Int. Biodeter. Biodegr.* **2017**, *125*, 258–268. [[CrossRef](#)]
17. Castañeda-Díaz, J.; Pavón-Silva, T.; Gutiérrez-Segura, E.; Colín-Cruz, A. Electrocoagulation-Adsorption to Remove Anionic and Cationic Dyes from Aqueous Solution by PV-Energy. *J. Chem.* **2017**, *2017*, 5184590. [[CrossRef](#)]
18. Kristianto, H.; Rahman, H.; Prasetyo, S.; Sugih, A.K. Removal of Congo red aqueous solution using *Leucaena leucocephala* seed's extract as natural coagulant. *Appl. Water Sci.* **2019**, *9*, 88. [[CrossRef](#)]
19. Gadekar, R.; Ahammed, M.M. Coagulation/flocculation process for dye removal using water treatment residuals: Modelling through artificial neural networks. *Desalin. Water Treat.* **2016**, *57*, 26392–26400. [[CrossRef](#)]
20. Lu, L.; Wu, J.; Wang, J.; Liu, J.Q.; Li, B.H.; Singh, A.; Kumar, A.; Batten, S.R. An uncommon 3D 3,3,4,8-c Cd(II) metal-organic framework for highly efficient luminescent sensing and organic dye adsorption: Experimental and theoretical insight. *CrystEngComm* **2017**, *19*, 7057–7067. [[CrossRef](#)]
21. Wang, C.K.; Xing, F.F.; Bai, Y.L.; Zhao, Y.M.; Li, M.X.; Zhu, S.R. Synthesis, structure of semi-rigid tetracarboxylate Cu(II) porous coordination polymers and their versatile high efficiency catalytic dye degradation in neutral aqueous solution. *Cryst. Growth Des.* **2016**, *16*, 2277–2288. [[CrossRef](#)]
22. Wang, X.; Ye, N. Recent advances in metal-organic frameworks and covalent organic frameworks for sample preparation and chromatographic analysis. *Electrophoresis* **2017**, *38*, 3059–3078. [[CrossRef](#)] [[PubMed](#)]
23. Uflyand, I.E.; Zhinzhiro, V.A.; Nikolaevskaya, V.O.; Kharisov, B.I.; Oliva González, C.M.; Kharissova, O.V. Recent strategies to improve MOF performance in solid phase extraction of organic dyes. *Microchem. J.* **2021**, *168*, 106387. [[CrossRef](#)]
24. Chui, S.S.-Y.; Lo, S.M.-F.; Charmant, J.P.H.; Guy Orpen, A.; Williams, I.D. A Chemically Functionalizable Nanoporous Material [Cu₃(TMA)₂(H₂O)₃]_n. *Science* **1999**, *283*, 1148–1150. [[CrossRef](#)]
25. Gascon, J.; Aguado, S.; Kapteijn, F. Manufacture of dense coatings of Cu₃(BTC)₂ (HKUST-1) on α -alumina. *Microporous Mesoporous Mater.* **2008**, *113*, 132–138. [[CrossRef](#)]
26. Mustafa, D.; Breyneart, E.; Bajpe, S.R.; Martens, J.A.; Kirschhock, C.E.A. Stability improvement of Cu₃(BTC)₂ metal-organic frameworks under steaming conditions by encapsulation of a Keggin polyoxometalate. *Chem. Commun.* **2011**, *47*, 8037–8039. [[CrossRef](#)]
27. Seo, Y.K.; Hundal, G.; Jang, I.T.; Hwang, Y.K.; Jun, C.H.; Chang, J.-S. Microwave synthesis of hybrid inorganic-organic materials including porous Cu₃(BTC)₂ from Cu(II)-trimesate mixture. *Microporous Mesoporous Mater.* **2009**, *119*, 331–337. [[CrossRef](#)]

28. Chen, J.; Yu, T.; Xiao, H.; Zhou, G.; Weng, L.; Tu, B.; Zhao, D. Synthesis and Structure of a New 3D Porous Cu(II)–Benzene-1,3,5-tricarboxylate Coordination Polymer, $[\text{Cu}_2(\text{OH})(\text{BTC})(\text{H}_2\text{O})]_n \cdot 2n\text{H}_2\text{O}$. *Chem. Lett.* **2003**, *32*, 590–591. [[CrossRef](#)]
29. Mao, Y.; Shi, L.; Huang, H.; Yu, Q.; Ye, Z.; Peng, X. Mesoporous separation membranes of $\{[\text{Cu}(\text{BTC}-\text{H}_2)_2 \cdot (\text{H}_2\text{O})_2] \cdot 3\text{H}_2\text{O}\}$ nanobelts synthesized by ultrasonication at room temperature. *CrystEngComm* **2013**, *15*, 265–270. [[CrossRef](#)]
30. Zornoza, B.; Seoane, B.; Zamaro, J.M.; Téllez, C.; Coronas, J. Combination of MOFs and zeolites for mixed-matrix membranes. *ChemPhysChem* **2011**, *12*, 2781–2785. [[CrossRef](#)]
31. Uflyand, I.E.; Naumkina, V.N.; Zhinzhiro, V.A. Nanocomposites of Graphene Oxide and Metal-Organic Frameworks. *Russ. J. Appl. Chem.* **2021**, *94*, 1453–1468. [[CrossRef](#)]
32. Zheng, M.; Xu, L.; Chen, C.; Labiadh, L.; Yuan, B.; Fu, M.-L. MOFs and GO-based composites as deliberated materials for the adsorption of various water contaminants. *Separ. Purif. Technol.* **2022**, *294*, 121187. [[CrossRef](#)]
33. Hummers, W.S., Jr.; Offeman, R.E. Preparation of Graphitic Oxide. *J. Am. Chem. Soc.* **1958**, *80*, 1339. [[CrossRef](#)]
34. Novikova, A.A.; Burlakova, V.E.; Varavka, V.N.; Uflyand, I.E.; Drozan, E.G.; Irkha, V.A. Influence of glycerol dispersions of graphene oxide on the friction of rough steel surfaces. *J. Mol. Liq.* **2019**, *284*, 1–11. [[CrossRef](#)]
35. Rauf, M.A. Solvatochromic behavior on the absorption and fluorescence spectra of Rose Bengal dye in various solvents. *Spectrochim. Acta Part A Mol. Biomol. Spectrosc.* **2009**, *72*, 133–137. [[CrossRef](#)]
36. Naser, J.A. Adsorption kinetic of malachite green dye from aqueous solutions by electrospun nanofiber Mat. *Orient. J. Chem.* **2017**, *33*, 3121–3129. [[CrossRef](#)]
37. Latif, I.K.; Abdullah, H.M.; Saleem, M.H. Magnetic conductive hydrogel nanocomposites as drug carrier. *Nanosci. Nanotechnol.* **2016**, *6*, 48–58.
38. Baidya, K.S.; Kumar, U. Adsorption of brilliant green dye from aqueous solution onto chemically modified areca nut husk. *S. Afr. J. Chem. Eng.* **2021**, *35*, 33–43.
39. Rehman, R.; Muhammad, S.J.; Arshad, M. Brilliant green and acid orange 74 dyes removal from water by Pinus roxburghii leaves in naturally benign way: An application of green chemistry. *J. Chem.* **2019**, *2019*, 3573704. [[CrossRef](#)]
40. Jaspal, D.; Malhotra, S.; Malviya, A. Column Studies for the Adsorption of Brilliant Green, Fast Green FCF and Phenol Red Dyes on De-Oiled Soya and Bottom Ash. *Asian J. Chem.* **2012**, *24*, 5082–5086.
41. Simonin, J.-P. On the comparison of pseudo-first order and pseudo-second order rate laws in the modeling of adsorption kinetics. *Chem. Eng. J.* **2016**, *300*, 254–263. [[CrossRef](#)]
42. Pehlivan, E.; Arslan, G. Comparison of adsorption capacity of young brown coals and humic acids prepared from different coal mines in Anatolia. *J. Hazard. Mater. B* **2006**, *138*, 401–408. [[CrossRef](#)] [[PubMed](#)]
43. Shahriary, L.; Athawale, A.A. Graphene oxide synthesized by using modified Hummers approach. *Int. J. Renew. Energy Environ. Eng.* **2014**, *2*, 58–63.
44. Lian, P.; Zhu, X.; Liang, S.; Li, Z.; Yang, W.; Wang, H. Large reversible capacity of high quality graphene sheets as an anode material for lithium-ion batteries. *Electrochim. Acta* **2010**, *55*, 3909–3914. [[CrossRef](#)]
45. Manoranjan, C.H.; Rosa, S.R.D.; Kottegoda, I.R.M. XRD-HTA, UV Visible, FTIR and SEM interpretation of reduced graphene oxide synthesized from high purity vein graphite. *Mater. Sci. Res. India* **2017**, *14*, 19–30. [[CrossRef](#)]
46. Seredych, M.; Petit, C.; Tamashausky, A.V.; Bandoz, T.J. Role of graphite precursor in the performance of graphite oxides as ammonia adsorbents. *Carbon* **2009**, *47*, 445–456. [[CrossRef](#)]
47. Domán, A.; Klébert, S.; Madarász, J.; Sáfrán, G.; Wang, Y.; László, K. Graphene Oxide Protected Copper Benzene-1,3,5-Tricarboxylate for Clean Energy Gas Adsorption. *Nanomaterials* **2020**, *10*, 1182. [[CrossRef](#)]